ResearchGate

See discussions, stats, and author profiles for this publication at: https://www.researchgate.net/publication/261137032

Modeling Swelling Behavior of Thermoresponsive Polymer Brush with Lattice Density Functional Theory

ARTICLE *in* LANGMUIR · MARCH 2014

Impact Factor: 4.46 · DOI: 10.1021/la5003429 · Source: PubMed

CITATIONS
9

READS
73

7 AUTHORS, INCLUDING:

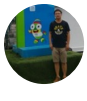

Cheng Lian
East China University of Science and Technology
10 PUBLICATIONS **41** CITATIONS
SEE PROFILE

Le Wang
316 PUBLICATIONS **2,883** CITATIONS
SEE PROFILE

Xia Han
shandong laiwu people hospital
51 PUBLICATIONS **414** CITATIONS
SEE PROFILE

Shuangliang Zhao
East China University of Science and Technology
35 PUBLICATIONS **174** CITATIONS
SEE PROFILE

Available from: Cheng Lian
Retrieved on: 02 February 2016

Langmuir

Article

pubs.acs.org/Langmuir

Modeling Swelling Behavior of Thermoresponsive Polymer Brush with Lattice Density Functional Theory

Cheng Lian,[†] Le Wang,[‡] Xueqian Chen,*[,§] Xia Han,[†] Shuangliang Zhao,[∥] Honglai Liu,*[,†] and Ying Hu[†]

[†]State Key Laboratory of Chemical and Engineering and Department of Chemistry, East China University of Science and Technology, Shanghai 200237, China

[‡]Department of Chemical and Biomolecular Engineering, Rice University, Houston, Texas 77005, United States

[§]Department of Physics, East China University of Science and Technology, Shanghai 200237, China

[∥]Department of Chemical Engineering, East China University of Science and Technology, Shanghai 200237, China

ABSTRACT: A key problem in designing thermoresponsive polymer brushes on a solid surface is to find a relation between the targeted thermoresponsive properties and controllable conditions. Usually, a temperature-thickness curve showing the heating-induced swelling behavior of polymer brushes is chosen as the relation by either experimental or theoretical investigation. In this work, a lattice density functional theory (LDFT) developed previously is employed to investigate the temperature-thickness curves for five different types of polymer brushes, where the density profiles of polymer brushes calculated by LDFT are compared directly with simulation. It is found that the thermoresponsive behavior of a polymer brush can be characterized by the bulk phase behaviors of its corresponding polymer solution, including UCST, LCST, both UCST and LCST, closed LOOP and hourglass-shaped, which implies that the bulk phase diagram of polymer solutions can help us to find an appropriate polymer brush for a targeted thermoresponsive behavior. As an example, we show that the swelling behavior of a thermoresponsive polymer brush found in the experiment could be predicted by our LDFT results with the bulk phase diagram of real polymer solution only.

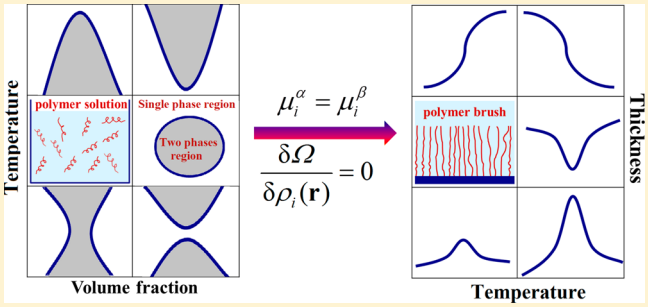

1. INTRODUCTION

Stimuli-responsive polymer materials, which can respond to various external signals from environmental adjustment (such as temperature, light, pH, solvent selectivity, electric field, etc.), have attracted attention in recent years and play an increasingly important role in a diverse range of applications, such as drug delivery, diagnostics, tissue engineering, and "smart" optical systems, as well as biosensors, coatings, and textiles.[1−3] In recent years, more and more attention has been paid to the polymer brushes grafted on a solid material surface as a candidate for smart surface. Polymer brushes have already shown various applications in nanotechnology and "smart" materials,[4−10] such as microfluidic channels, environment-responsive lithography, "smart" coatings, responsive colloids, protein adsorption, etc.

To design polymer-brush-based thermoresponsive surfaces, it is necessary to investigate first the influence of grafting density, polymer chain length, and all intermolecular or intramolecular interactions on the heating-induced swelling behavior of polymer brushes. In practice, it is advisable to simplify the investigation by starting from checking its corresponding bulk system. It is well-known that the information on the heating-induced phase transition of a polymer solution, primarily a phase diagram, can be characterized by its critical solution temperature such as the lower critical solution temperature (LCST) or the upper critical solution temperature (UCST). A specific bulk phase diagram is expected to generate a specific swelling behavior of its corresponding inhomogeneous brush system.

There have been several experimental efforts to study the swelling behavior of polymer brushes. As a kind of thermoresponsive polymers, poly(*N*-isopropylacrylamide) (PNIPAM) undergoes a sharp conformational change near the lower critical solution temperature (LCST) of 32 °C. Below the LCST, the PNIPAM chains are hydrophilic and extended in water. Above the LCST, the PNIPAM chains become hydrophobic and collapse to avoid contact with water. For the PNIPAM brushes prepared on a solid substrate, the temperature-driven collapse transition only happens at the higher grafting density and higher molecular mass.[11−14] For upper critical solution temperature (UCST) systems, the polymer chains are hydrophilic above the UCST and hydrophobic below the UCST. After grafting this kind of polymer chains onto a solid surface, generally there is a continuous decrease in polymer film thickness as the temperature is lowered.[15] LCST or UCST polymer brushes have been extensively investigated by experiments. However,

Received: February 10, 2014
Revised: March 11, 2014
Published: March 26, 2014

 © 2014 American Chemical Society dx.doi.org/10.1021/la5003429 | *Langmuir* 2014, 30, 4040−4048

the experimental investigation for polymer brush system with both LCST and UCST is not found.[4,16,17]

The swelling behavior of polymer brushes has also been studied with molecular simulations. Amitabha and co-workers studied a system with a large number of polymer chains terminally anchored on a flat surface by a three-dimensional lattice Monte Carlo method. They found a depletion layer near the grafting plane, and the density profile exhibits a parabolic form.[18] Lai and Binder[19] used the Monte Carlo method to study polymer brushes in various solvent qualities. They found a continuous decrease of the first moment of the segment density profile with the decrease of temperature. And, under poor solvent conditions, they observed lateral heterogeneities in the film. Grest et al.[20−24] modeled polymer brushes with explicit or implicit solvent for a range of solvent qualities using molecular dynamics (MD) simulations and studied the effect of solvent on the brush. It is very difficult for molecular simulation to obtain the relationship between the polymer brush conformation change and the bulk phase diagram of polymer solutions. Lee et al.[25] reported MD simulations to show the deswelling mechanisms of the hydrated surface-grafted PNIPAM brush at various temperatures. They observed that, at the temperatures above LCST (∼305 K), the water molecules are departed from the brush to form separated water phase, and simultaneously, the brush is collapsed. The phenomena were not observed at the temperatures below LCST. From these results, they found that the LCST of the PNIPAM brush is driven by the entropic contribution. Apart from polymer brushes with LCST, there are barely any simulation works, concerning the relationship between the polymer brush conformation change and the bulk phase diagram of polymer solutions.

Various theoretical approaches have been used to understand the equilibrium structure of planar brushes, especially the LCST behavior of polymer brushes. Alexander[26] and de Gennes[27] developed scaling theories for brushes. At low grafting densities, each chain is isolated, occupying roughly a half-sphere with a radius comparable to the radius of gyration ("mushroom" regime); at high grafting densities, polymers stretch away from the interface to avoid overlapping, forming a polymer "brush", and these scaling theories could describe the LCST behavior of brushes quantitatively. In addition, self-consistent field theory (SCFT) has been used for the brushes by various researchers.[28−34] Sergio and co-workers modeled the effects of temperature on the LCST behavior of the PNIPAM brush in water by a numerical SCFT method, an empirical χ parameter obtained from the bulk phase diagram of PNIPAM solutions was used as the input of their theory. At low temperatures, the composition profiles are approximately parabolic and extend into the solvent. In contrast, at temperatures above the LCST of the bulk solution, the polymer profiles are collapsed near the surface. To describe the brush systems, classical density functional theory (DFT) has been proven to be robust.[10,35−38] However, among these DFT work, only Gong[38] studied the LCST behavior of the PNIPAM brush in water using classical density functional theory. By modeling the hydrogen-bonding interactions between polymer and solvent, they found the phase transition of polymer brushes from extended to collapsed structure with increasing temperature, indicating the LCST behavior of polymer brushes. Most theories studying the brush conformation change of thermoresponsive polymers brushes focused on the LCST behavior of brushes, only a very few works were concerned on other thermoresponsive polymers brushes.

It is well-realized that the LCST or UCST phase behaviors of polymer solution result from the competition between the nonpolar and polar interactions (such as hydrogen bond). In this work, a lattice density functional theory (LDFT), considering the counterbalance between entropy and enthalpy, including the contribution from chain connectivity and nonpolar or polar interactions, is used to link the heat-induced conformational response of the polymer brush to the bulk phase diagram of its corresponding polymer solution.

LDFT has several advantages over more complicated free space DFT such as mathematical simplicity of lattice model (compared to free space model) and ease of incorporating complex boundary conditions. Although this approach is known to give only coarse-grained information about the thermodynamic behavior of a system, it provides important insights on the mechanisms of various complex phenomena such as phase transition,[39] configurationally distribution,[40] surface adsorption,[41] and crystallization.[42] In our previous work,[41] a LDFT for polymer solutions is constructed by adopting the close-packed molecular thermodynamic model[43−45] for polymer solutions with local density approximation (LDA) and weighted density approximation (WDA). To the best of our knowledge, no LDFT has been developed for polymer brushes. In this work, we plan to extend LDFT to study the thermoresponsive polymer brush. Five types of homopolymer brushes characterized by different phase diagrams will be discussed to show the correspondence between polymer solution's bulk phase behavior and the swelling behavior of brushes. With the help of this correspondence, we can predict the tethered PNIPAM brush with the phase behavior of the bulk polymer solutions only as input. This paper is organized as follows: Section 2 presents the LDFT for thermoresponsive polymers, Section 3 shows results and corresponding discussion, and Section 4 contains concluding remarks.

2. THEORY

2.1. Model. Homopolymer brushes with chain length r in different solvents at different temperatures are considered. They are modeled as freely jointed chains with one end tethered to a surface in the framework of the LDFT. To graft polymers onto a surface, a bonding potential between the first segment of homopolymers and the surface is considered, which is given by

$$V_1^{\text{ext}}(z) = \begin{cases} -\infty, & z = 0 \\ 0, & \text{otherwise} \end{cases} \quad (1)$$

where z is the distance (or the number of lattices) between the polymer segment and the surface. The interaction between the surface and the other chain segments is treated as a wall without interaction

$$V_i^{\text{ext}}(z) = 0,\ i = 2, \ldots, r \quad (2)$$

The other situations of the substrate are discussed later in Section 3.

2.2. Lattice Density Functional Theory. We consider the homopolymer brushes composed of r segments in the solvent with a chain length of 1. A lattice DFT based on a close-packed lattice[43−45] is formulated for an open system in the grand

dx.doi.org/10.1021/la5003429 | Langmuir 2014, 30, 4040−4048

canonical ensemble. In the LDFT, the grand potential Ω can be expressed as a functional of the density profile,

$$\Omega[\rho_s, \rho_p] = F[\rho_s, \rho_p] + \sum_j \int [V_j^{ext}(\mathbf{Q}_j) - \mu_j]\rho_j(\mathbf{Q}_j)\, d\mathbf{Q}_j \tag{3}$$

where the subscripts s and p stand for solvent and homopolymer, μ_j and V_j^{ext} are the chemical potential and the external field exerted on the component j, respectively. $\mathbf{Q}_p = (\boldsymbol{q}_1, \boldsymbol{q}_2, \mathbf{L}, \boldsymbol{q}_r)$ denotes the conformation of a polymer chain with chain length r in lattice and $\mathbf{Q}_s = \boldsymbol{q}$ for a solvent. F is the intrinsic Helmholtz free-energy functional, which can be separated into two contributions: the ideal part and the excess part

$$F[\rho_p(\mathbf{Q}), \rho_s(\mathbf{q})] = F^{id}[\rho_p(\mathbf{Q}), \rho_s(\mathbf{q})] + F^{ex}[\rho_p(\mathbf{Q}), \rho_s(\mathbf{q})] \tag{4}$$

$$\begin{aligned}\beta F^{id}[\rho_p(\mathbf{Q}), \rho_s(\mathbf{q})] &= \sum_Q \rho_p(\mathbf{Q}) \ln \rho_p(\mathbf{Q}) + \sum_q \rho_s(\mathbf{q}) \ln \rho_s(\mathbf{q}) \\ &\quad + \beta \sum_Q \rho_p(Q) V_{int}(\mathbf{Q})\end{aligned} \tag{5}$$

where $\beta = 1/k_BT$, k_B is the Boltzmann constant, T is the temperature and V_{int} is the intermolecular interaction of the polymer chains.

The excess part is approximated as a functional of solvent density distribution $\rho_s(\boldsymbol{q})$ and the average segment-density distribution $\rho_m(\boldsymbol{q})$. The latter is related to polymer density $\rho_p(\mathbf{Q})$ via a transform as

$$\rho_m(\mathbf{q}) = \sum_{\mathbf{Q}} \sum_{j=1}^{r} \delta(\mathbf{q}_j - \mathbf{q})\rho_p(\mathbf{q}) \tag{6}$$

where $\delta(x)$ is a Kronecker delta, $\delta(x) = \delta_{0x}$. For a close-packed lattice model, the polymer solution is incompressible,

$$\rho_m(\mathbf{q}) + \rho_s(\mathbf{q}) = 1 \tag{7}$$

To construct the excess Helmholtz energy functional F^{ex} for inhomogeneous fluids, the close-packed molecular thermodynamic model for homogeneous bulk fluids is used by combining the LDA and nonlocal WDA. The excess Helmholtz energy functional is then separated into the athermal entropy of mixing and the internal energy of mixing.

$$\begin{aligned}F^{ex}[\rho_p(\mathbf{Q}), \rho_s(\mathbf{q})] &= F_{ather}[\rho_p(\mathbf{Q}), \rho_s(\mathbf{q})] \\ &\quad + F_{inter}[\rho_p(\mathbf{Q}), \rho_s(\mathbf{q})]\end{aligned} \tag{8}$$

This athermal excess Helmholtz energy functional can be estimated via the Staverman−Guggenheim athermal entropy of mixing,[46]

$$\beta F_{ather}[\rho_p(\mathbf{Q}), \rho_s(\mathbf{q})] = \sum_q \phi_{ch}[\rho_p(\mathbf{Q}), \rho_s(\mathbf{q})] \tag{9}$$

where ϕ_{ch} is a function of $\rho_m(\boldsymbol{q})$ and $\rho_s(\boldsymbol{q})$, representing the segment−segment (intrachain or interchain) and segment−solvent volume repulsions in athermal solution.

$$\phi_{ch}(\rho_m, \rho_s) = \frac{Z_c}{2}\left[\frac{q_r}{r}\rho_m \ln \frac{q_r}{r} - \left(\frac{q_r}{r}\rho_m + \rho_s\right) \ln\left(\frac{q_r}{r}\rho_m + \rho_s\right)\right] \tag{10}$$

where $q_r = [(Z_C - 2)r + 2]/Z_C$. The approximate density functional of the internal energy of mixing could be obtained by WDA,

$$F_{inter}[\rho_p(\mathbf{Q}), \rho_s(\mathbf{q})] = \sum_q \rho_m(\mathbf{q}) f_{inter}[\overline{\rho}_p(\mathbf{q}), \overline{\rho}_s(\mathbf{q})] \tag{11}$$

Where $\overline{\rho}_p(\boldsymbol{q})$ and $\overline{\rho}_s(\boldsymbol{q})$ are the weighted densities defined as

$$\overline{\rho}_m(\mathbf{q}) = \sum_{\mathbf{q}'} w(|\mathbf{q}' - \mathbf{q}|)\rho_m(\mathbf{q}') \tag{12}$$

$$\overline{\rho}_s(\mathbf{q}) = 1 - \overline{\rho}_m(\mathbf{q}) \tag{13}$$

The internal energy of mixing f_{inter} could be further decomposed into two contributions,[19] the attractive interactions and the coupling effects between energetic correlation and chain connectivity, respectively.

$$f_{inter}[\rho_s, \rho_m] = f_{am}[\rho_s, \rho_m] + f_{ac}[\rho_s, \rho_m] \tag{14}$$

The expressions of the two functions, f_{inter} for the attractive interactions and f_{ac} for the coupling effects, can be obtained through the Helmholtz energy for uniform fluids,

$$f_{am}[\rho_s, \rho_m] = \frac{Z_C}{2}\left[\tilde{\varepsilon}\rho_s - \frac{1}{2}\tilde{\varepsilon}^2\rho_m\rho_s^2 - \frac{1}{2}\tilde{\varepsilon}^3\rho_m\rho_s^2 (1 - 2\rho_m\rho_s)\right] \tag{15}$$

$$f_{ac}[\rho_s, \rho_m] = -\frac{r - 1 - \lambda}{r} \ln \frac{[\exp(\tilde{\varepsilon}) - 1]\rho_s + 1}{[\exp(\tilde{\varepsilon}) - 1]\rho_s\rho_m + 1} \tag{16}$$

where $\tilde{\varepsilon}$ represents the attraction interactions between the nearest-neighbor sites, which is a reduced exchange energy, $\tilde{\varepsilon} = (\varepsilon/kT) = [(\varepsilon_{pp} + \varepsilon_{ss} - 2\varepsilon_{ps})/kT]$ between segment p and solvent s, where ε_{ij} is the attractive energy of the i−j pair. And λ is a factor accounting for the long-range correlations of polymers defined as

$$\lambda = \frac{(r - 1)(r - 2)}{r^2}(ar + b) \tag{17}$$

In this work, we use the Heaviside step function to estimate the weighted densities. The attraction exists between the nearest neighbors only; therefore, the weighting summation constrained by the Heaviside step function Θ merely runs over the sites adjacent to the site $\boldsymbol{q}$ and itself. The weighting function is given by

$$w(x) = \frac{\Theta(x - 1)}{Z_C + 1} \tag{18}$$

By minimizing the grand free energy with respect to the density profile, the equilibrium density distribution of segments can be obtained,

$$\frac{\delta\Omega}{\delta\rho_p} = 0 \tag{19}$$

And the Euler−Lagrange equations are yielded

dx.doi.org/10.1021/la5003429 | Langmuir 2014, 30, 4040−4048

$$\rho_p(\mathbf{Q}) = \exp[\beta\mu_p - \beta V_{int}(\mathbf{Q}) - \beta\Psi(\mathbf{Q})] \quad (20)$$

where

$$\beta\Psi(\mathbf{Q}) = \sum_{j=1}^{r} \beta\varphi(\mathbf{q}_j) = \sum_{j=1}^{r}\left[\frac{1}{r} - 1 - \ln \rho_s(\mathbf{q}_j) + \frac{\delta\beta F^{ex}}{\delta\rho_p(\mathbf{q}_j)} + V_i^{ext}\right] \quad (21)$$

And the Euler−Lagrange equations [eqs 20)] can be further simplified to

$$\rho_m(\mathbf{q}) = \sum_{\mathbf{Q}}\sum_{j=1}^{r} \delta(\mathbf{q}_j - \mathbf{q})\exp[\beta\mu_p - \beta V_{int}(\mathbf{Q}) - \beta\Psi(\mathbf{Q})] \quad (22)$$

Considering the bonding potential between the nearest neighbor segments, a numerical solution is adopted as

$$\rho_m(\mathbf{q}) = \sum_{j=1}^{r} \exp[\beta\mu_p - \beta\Psi(\mathbf{Q})]G_L^{(j)}(\mathbf{q})G_R^{(j)}(\mathbf{q}) \quad (23)$$

where

$$G_L^{(j)}(\mathbf{q}) = \sum_{\mathbf{Q}} \frac{\delta(|\mathbf{q}' - \mathbf{q}| - 1)}{Z_C}\exp[\beta\varphi(\mathbf{q}')]G_L^{(j-1)}(\mathbf{q}') \quad (24)$$

$$G_R^{(j)}(\mathbf{q}) = \sum_{Q} \frac{\delta(|\mathbf{q}' - \mathbf{q}| - 1)}{Z_C}\exp[\beta\varphi(\mathbf{q}')]G_R^{(j+1)}(\mathbf{q}') \quad (25)$$

where $j = 1, 2, ..., r-1$, and $G_L^{(1)}(\mathbf{q})\ G_R^{(r)}(\mathbf{q}) = 1$.

We solve the density distributions of polymer segments using the Picard iteration method. The numerical procedure starts with an initial guess for the density profiles of polymer based on their bulk densities. The iterations are repeated until the convergence criterion is satisfied (typically $|\rho_{new} - \rho_{old}| <$ tolerance). And the average thickness of the polymer brushes $\langle H\rangle$ can be described by twice the first moment of the density distribution,

$$\langle H\rangle = \frac{2\int z\rho(z)\,dz}{\int \rho(z)\,dz} \quad (26)$$

3. RESULTS AND DISCUSSIONS

3.1. Comparison between MC and LDFT Results. We validate the numerical performance of the lattice density functional theory (LDFT) with molecular simulations for plat homopolymer brushes in athermal and thermal solvents. We compare the density profiles of polymer segments calculated by LDFT with reported Monte Carlo (MC) simulations.

We first consider the case of pure athermal polymer chains at a planar surface, the exchange energy $\tilde{\varepsilon}$ is set to be zero, and the interaction between the surface and nongrafting segments is ignored. The monomer density as a function of distance z from the grafting plane, for several values of the surface coverage σ, is shown in Figure 1 (panels a and b), with chain lengths $r = 49$ and $r = 99$. For all values of σ considered here, the density profile obtained from LDFT shows a maximum (depletion layer) close to the grafting surface in agreement with MC simulation results.[18]

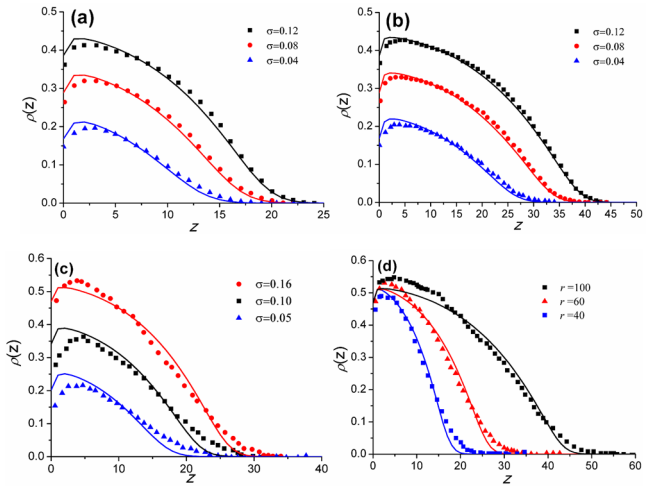

Figure 1. Density profile as a function of the distance from the grafting plane, z. (a and b) for several values of the surface coverage when the exchange energy $\tilde{\varepsilon}$ is zero: (a) polymer brush chain length $r = 49$ and (b) $r = 99$. (c) The brush polymer length $r = 60$, and the exchange energy $\tilde{\varepsilon} = 0.5$. (d) Corresponds to $\sigma = 0.16$ and $\tilde{\varepsilon} = 0.5$ with different chain lengths $r = 40$, 60, and 100. These points are simulation results and lines are calculated by our LDFT.

Figure 1 (panels c and d) show several density profiles for $\tilde{\varepsilon} = 0.5$ obtained from our LDFT calculation and reported simulation results[47] for different surface densities and polymer chain lengths. Our results are in good agreement with those of MC simulation, but with small discrepancies near the grafting surface, which can be ascribed to the presence of fluctuations in the simulations resulting from finite chains. In particular, we found that some physical quantities, such as the density profile and the profile of end segments of homopolymer chains of the brush, compare well with the results of MC simulation. The agreement of physical quantities between LDFT and MC simulation is good for both cases, and the LDFT shows good numerical performance on the prediction of the density profiles.

3.2. Thermoresponsive Brushes. It has been found that the lattice model in this work can accurately describe all five types of phase diagrams of binary polymer solutions, such as UCST, LCST, both UCST and LCST, closed LOOP, and hourglass shaped. These phase diagrams can be characterized by the exchange energy, based on the idea of the double lattice model,[48−51] as follows

$$\tilde{\varepsilon} = \sum_i \frac{\varepsilon_i}{(kT_r)^i},\ i = 1, 2, 3... \quad (27)$$

where ε_i is the energy parameter and $T_r = T/100$. And the relationship between the energy parameters and the phase diagrams of binary polymer solutions containing the information on all the nonpolar interactions and polar interactions can be found in previous papers.[43−45,52,53]

Here, we study the effects of polymer solution's phase behavior on the swelling behavior of brushes to show how the temperature affects the equilibrium structure of the polymer brushes. Five types of homopolymer brushes with different phase diagrams are discussed.

First, coexistence curves for polymer solutions are obtained by chemical potential equalities:

dx.doi.org/10.1021/la5003429 | Langmuir 2014, 30, 4040−4048

$$\mu_p^{(\alpha)} = \mu_p^{(\beta)}, \quad \mu_s^{(\alpha)} = \mu_s^{(\beta)} \tag{28}$$

Then the density profiles of polymer segments and the average thickness of polymer brushes are calculated by LDFT with the model parameters. Here, we fix the chain length r to be 50 and grafting densities σ to be 0.10, so that we can focus on the effects of temperature on the equilibrium structure of tethered polymer chains immersed in solvents without considering the effects of degree of polymerization (chain length) and surface coverage.

Figure 2 shows an example of polymer solutions with UCST and the equilibrium structure of tethered polymer chains

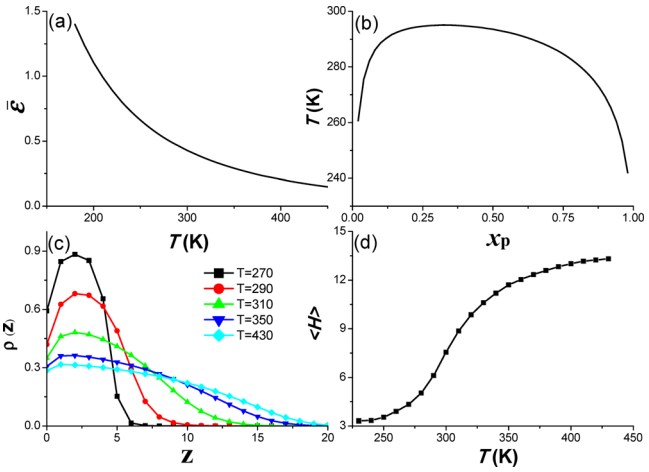

Figure 2. An example of polymer solution with UCST and the equilibrium structure of tethered polymer chains immersed in the same solvent. For both the bulk polymer solution and the tethered polymer brush system, the energy parameters are set to be $\varepsilon_1/k = -0.57$ K and $\varepsilon_2/k^2 = 5.56$ K^2, and the polymer chain length r is 50. And the surface coverage, $\sigma = 0.1$ for polymer brushes. (a) The reduced exchange energy as a function of temperature. (b) Coexistence curves of bulk polymer solutions with UCST, x_p is the mole fraction of polymer. (c) Density profile of polymer brushes as a function of the distance from the grafting plane z under different temperatures. (d) The average thickness of the brushes versus temperature T.

immersed in the same solvent under different temperatures. In accordance with our previous work, the reduced energy parameter could be expressed by two energy parameters. Here, we take $\varepsilon_1/k = -0.57$ K and $\varepsilon_2/k^2 = 5.56$ K^2. With eq 27, the relationship between $\tilde{\varepsilon}$ and temperature is shown in Figure 2a. $\tilde{\varepsilon}$ decreases as temperature increases, it means polymer and solvent are miscible at high temperature and immiscible at low temperature. We can also get this point from the phase diagram of polymer solution in Figure 2b. As shown from Figure 2 (panels c and d), at low temperature, the brush concentrated on the surface and transit to the mushroom regime due to the immiscibility. On the other hand, the chains become more stretched away from the substrate at high temperature. The results indicate that the average thickness $\langle H \rangle$ increases gradually with increasing temperature due to the increasing solvent quality or miscibility.

For the polymer solutions exhibit an LCST phase behavior, we use three model parameters $\varepsilon_1/k = 6.50$ K and $\varepsilon_2/k^2 = -13.5$ K^2 to get the phase diagram shown as Figure 3b. At low temperature, the polymers dissolve in water and form a homogeneous solution. At high temperature, the solution separates into two liquid phases with different polymer

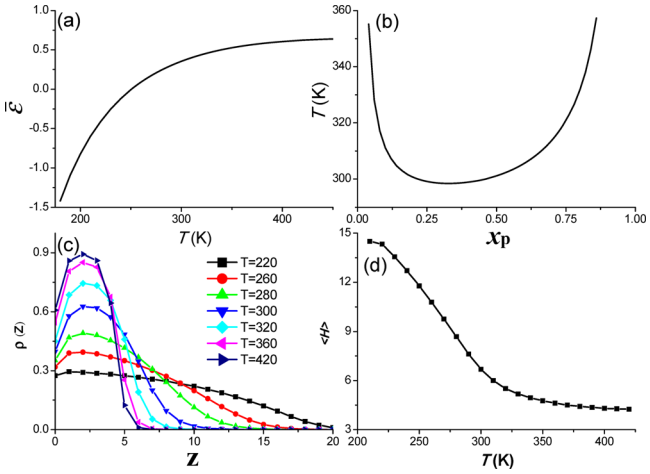

Figure 3. A polymer solution with LCST and its phase behavior under tethering constraint. The chain length $r = 50$, and reduced energy parameters $\varepsilon_1/k = 6.50$ K and $\varepsilon_2/k^2 = -13.5$ K^2. (a) The reduced exchange energy as a function of temperature. (b) Phase diagram of bulk polymer solutions with LCST, x_p is the mole fraction of polymer. (c) Density profile of polymer brushes as a function of the distance from the grafting plane z under different temperatures. (d) The average thickness of the brushes versus temperature T.

concentrations. The relationship between $\tilde{\varepsilon}$ and temperature is shown in Figure 3a. $\tilde{\varepsilon}$ increases as temperature increases. Using this relationship as input to our LDFT, the equilibrium structure of tethered polymer chains immersed in the solvent under different temperatures are calculated, as shown in Figure 3 (panels c and d). In contrast with the UCST situation, at a low temperature (below the transition temperature), the chains become more stretched away from the substrate and at a high temperature, the brush changes to the mushroom regime to minimize contact with the solvent. Thickness $\langle H \rangle$ of the brushes decreases with the increasing temperature due to the decreasing compatibility of the polymer and the solvent.

Figure 4 shows the polymer solutions exhibiting both LCST and UCST phase behavior and its phase behavior under tethering constraint. We use three model parameters, which are $\varepsilon_1/k = 12.0$ K, $\varepsilon_2/k^2 = -72.0$ K^2, and $\varepsilon_3/k^3 = 107.52$ K^3 to obtain reduced exchange energy under a different temperature, shown as Figure 4a. The reduced exchange energy $\tilde{\varepsilon}$ decreases with the increasing of temperature and then increases. And polymer and solvent are miscible at high temperature and immiscible at low temperature, shown as Figure 4b. The density distributions and average thickness of the brushes composed of this polymer solution are shown in Figure 4 (panels c and d). Unlike brushes having single LCST or UCST, at low temperature below the UCST or at high temperature above the LCST, the polymer brush changes to the mushroom regime in an attempt to minimize contact with the solvent; and at a specific temperature between the UCST and LCST, the brushes become most stretched to the maximum to contact the solvent. Below this specific temperature, the thickness of the brushes increases with the increasing temperature because of the increasing compatibility of the polymer and the solvent; and the thickness of the brushes decreases with the increasing temperature above the specific temperature.

Polymer solution with a miscibility loop phase diagram is shown in Figure 5b; at high or low temperature, the polymer becomes miscible with solvent, and the loop phase diagram can be obtained with the relationship between $\tilde{\varepsilon}$ and T shown as

dx.doi.org/10.1021/la5003429 | Langmuir 2014, 30, 4040−4048

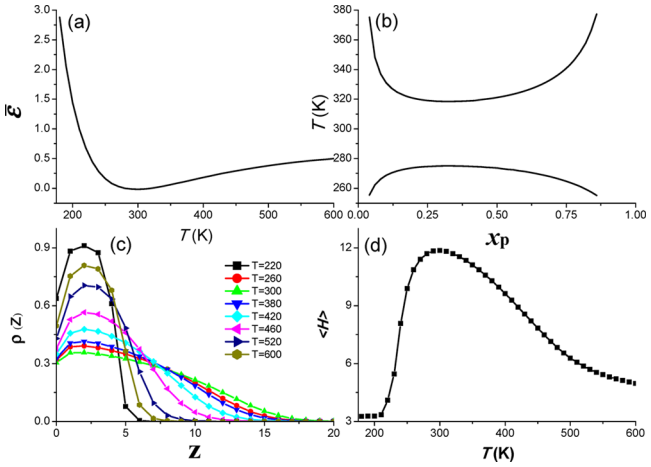

Figure 4. A polymer solution with both LCST and UCST and its phase behavior under tethering constraint. The chain length $r = 50$, $\varepsilon_1/k = 12.0$ K, $\varepsilon_2/k^2 = -72.0$ K^2, and $\varepsilon_3/k^3 = 107.52$ K^3. (a) The reduced exchange energy as a function of temperature. The reduced exchange energy $\tilde{\varepsilon}$ decreases with the increasing of temperature and then increases. (b) Coexistence curves of bulk binary polymer solutions with both UCST and LCST. (c) Density profile as a function of the distance from the grafting plane z under different temperatures, and the polymer brushes surface coverage $\sigma = 0.1$. (d) The swelling behavior of this kind of polymer brushes with varying temperature.

Figure 5a with three model parameters: $\varepsilon_1/k = -0.9$ K, $\varepsilon_2/k^2 = 14.4$ K^2, and $\varepsilon_3/k^3 = -21.22$ K^3. And the density distributions and average thickness of the brushes composed of this polymer and solvent are shown in Figure 5 (panels c and d). In contrast with the situation with both UCST and LCST, at low and high temperatures, the brushes are stretched to solvent and the average thickness reaches its maximum. Between the maximum and minimum temperatures in the loop phase diagram, the brush changes to mushroom regime to minimize contact with the solvent.

Figure 6 shows the polymer solutions exhibit an hourglass shape phase diagram. It is hourglass-shaped without critical point and phase separation occurs over the entire range of temperatures, as shown in Figure 6b. In accordance with our analysis above, it is obvious that the value of reduced energy is large because of the immiscibility. Four adjustable energy parameters have to be selected for this kind of phase diagram. They are $\varepsilon_1/k = 11.9$ K, $\varepsilon_2/k^2 = -7.3$ K^2, $\varepsilon_3/k^3 = -139.02$ K^3, and $\varepsilon_4/k^4 = 222.3$ K^4, with $r = 50$. And the density distributions of the brushes composed of this polymer solution are shown in Figure 6c. As shown in Figure 6d, the brushes gather on the surface so that the polymer that does not like the solvent can escape solvent contact at all temperatures. The average thickness, about 4.2−7.1 unit lengths, is smaller than these polymers that can be miscible in solutions (more than 10 unit length). From Figure 6c, we can find the thickness reaches its maximum at about 230 K. It is greatly bucked to find the answer from Figure 6 (panels a and b), the reduced energy reaches it minimum at 230 K, and this polymer is more miscible at 230 K than other temperatures despite not liking this solvent.

3.3. Application to Practical Systems. In this work, the method mentioned above is applied to obtain the density profiles of PNIPAM brushes in aqueous solution. The inputs in this LDFT are polymer chain length (r), the length of one lattice site (d), the reduced exchange energy ($\tilde{\varepsilon}$), and grafting densities (ρ_g), which is the number of freely jointed chains per unit area.

Here we specify how to place all molecules on a lattice and compute the reduced energy parameter between the polymer and solvent. For the PNIPAM/water mixture of interest we assume a water molecule occupies one lattice site. Hence we identify the size of one lattice site with the size of a water

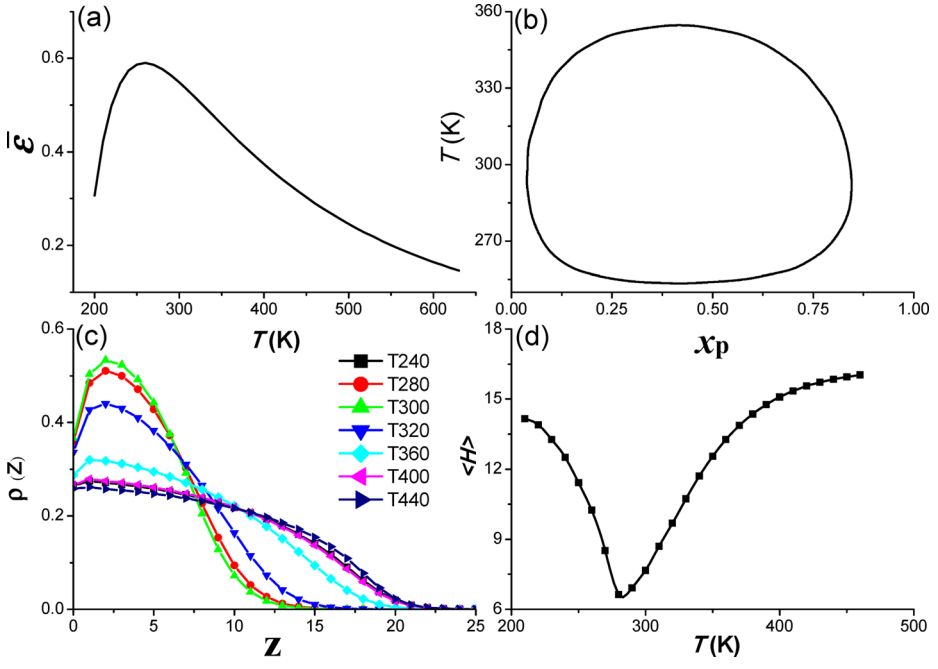

Figure 5. An example of polymer solution exhibits a closed-miscibility loop phase behavior and the phase behavior of its brushes. (a) The reduced exchange energy as a function of temperature. (b) A miscibility loop phase diagram is obtained with four model parameters: $r = 50$, $\varepsilon_1/k = -0.9$ K, $\varepsilon_2/k^2 = 14.4$ K^2, and $\varepsilon_3/k^3 = -21.22$ K^3. (c) Density profile of this tethered polymer as a function of the distance from the grafting plane z under varying temperatures, and the surface coverage σ is 0.1. (d) The average thickness of the brushes versus temperature.

dx.doi.org/10.1021/la5003429 | Langmuir 2014, 30, 4040−4048

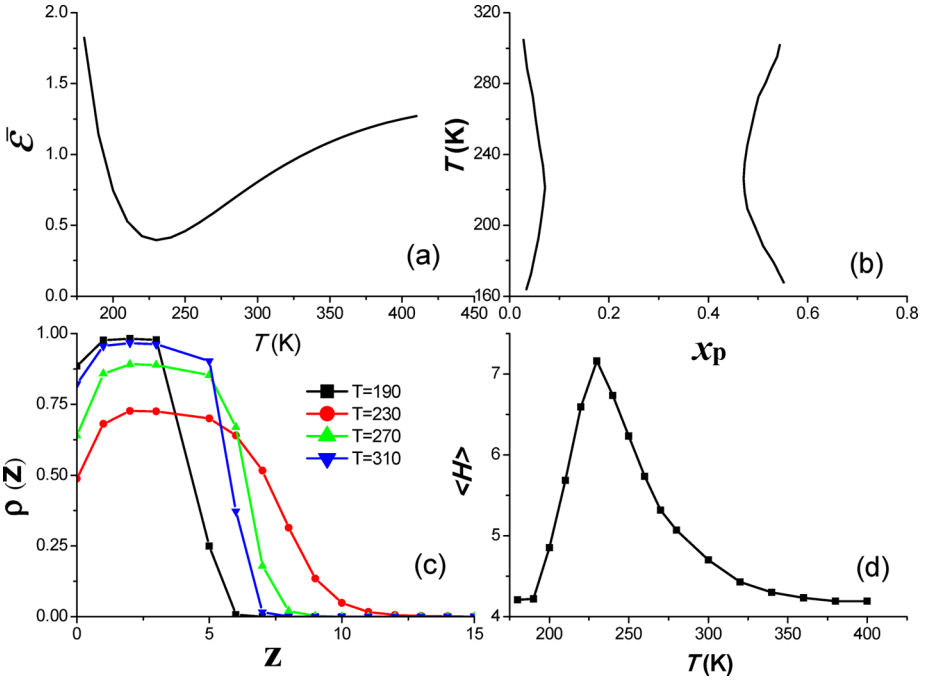

Figure 6. The polymer solutions exhibit an hourglass shape phase behavior and the thermoresponsive swelling behavior of this tethered brush. (a) The reduced exchange energy as a function of temperature with r = 50, ε_1/k = 11.9 K, ε_2/k^2 = −7.3 K^2, ε_3/k^3 = −139.02 K^3, and ε_4/k^4 = 222.3 K^4. (b) An hourglass-shaped phase diagram is obtained with the relationship in (a). (c) Profile of this tethered polymer near the surface as a function of the distance from the grafting plane z under varying temperatures. (d) The temperature sensitive swelling behavior of this tethered polymer. And for polymer brushes, the surface coverage σ is 0.1.

molecule. The size of one lattice site is then fixed; it is derived from the density of water. The density of water is 1000 kg/m^3. The molar mass of water is 18.0 g/mol, so the volume per molecule is about 2.99 × 10^{-29} m^3, which means one lattice site has a length d of 0.31 nm. The density of bulk PNIPAM is 1.1 g/cm^3. The molar mass of monomer is 113 g/mol, and it is easy to find the length of monomer, 0.55 nm, so that the chain length r in our model based on the molecular mass of the PNIPAM chain is fixed differently.

Then, the reduced exchange energy parameters are estimated from the experimental phase diagram for aqueous PNIPAM solutions from Afroze and his co-workers[54] by using eq 27. In accordance with the experimental data in Figure 7, the bimodal line and critical point are calculated with three parameters: the molecular mass (124 kg/mol) in the experiment means the chain length r in our lattice model is 1946, and the energy parameters are 7.50 K and −22.41 K^2 for the PNIPAM/water mixture.

With these energy parameters as input, the LDFT developed here could be used to obtain the heating-induced swelling behavior of two kinds of PNIPAM brushes with different polymer surface coverage from ref 11. The molecular characteristics of the two brush samples are studied here, both of them are with M_w = 47.6 kg/mol, r = 747. However, the grafting densities are different, ρ_g = 0.33 nm^{-2} for brush 1 and ρ_g = 0.11 nm^{-2} for brush 2.

Figure 8 shows the density profiles and the profiles of the free ends of the brush 1 under different temperatures. As shown in Figure 8, the composition profiles extend into the solvent at low temperatures because PNIPAM chains are more miscible below the LCST of the bulk solution. In contrast, at temperatures above the LCST of the bulk solution, polymer

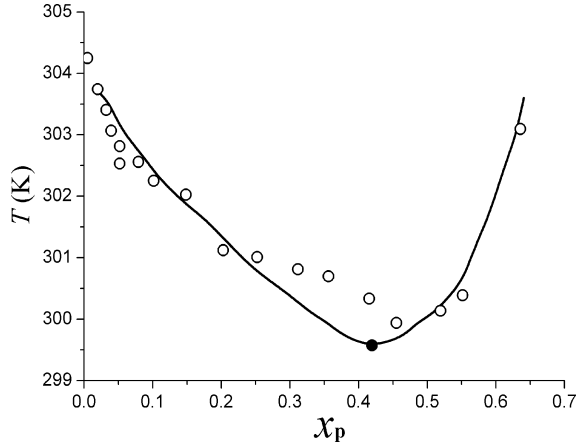

Figure 7. Phase diagram for aqueous PNIPAM solutions. These open circles (○) are experimental results of Afroze et al.[54] The solid curve is the bimodal line calculated by our lattice model with three parameters: r = 1946, the energy parameters are 7.50 and −22.41 K^2, and the point (●) is the critical point.

brushes are collapsed near the surface minimizing the contact with the solvent.

The experimental and calculated height changes of brushes 1 and 2 are shown in Figure 9, as we can see, the calculated results by LDFT in this work are qualitatively consistent with experiments, the height of both kinds of PNIPAM brushes decreases with increasing temperature. The swelling ratio of brush 1 with a higher grafting density (0.33 nm^{-2}) is 3.25, while the value of brush 2 is about 5.0. It seems that there is a less collective behavior of the PNIPAM chains due to the reduced interchain interactions at lower grafting densities, so that

dx.doi.org/10.1021/la5003429 | Langmuir 2014, 30, 4040−4048

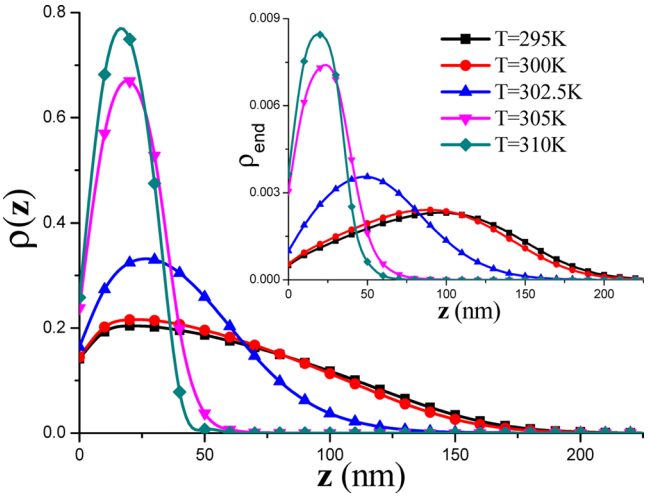

Figure 8. The density profiles of the brush 1 under different temperatures, with grafting density ρ_g = 0.33 nm^{-2}, molecular weight is 47.6 kg/mol which can be converted simply into model parameters: r = 747. The energy parameters are obtained from phase diagram for aqueous PNIPAM; they are ε_1/k = 7.50 K and ε_2/k^2 = −22.41 K^2. The inset shows the profiles of the free ends of the brush 1, with varying temperatures.

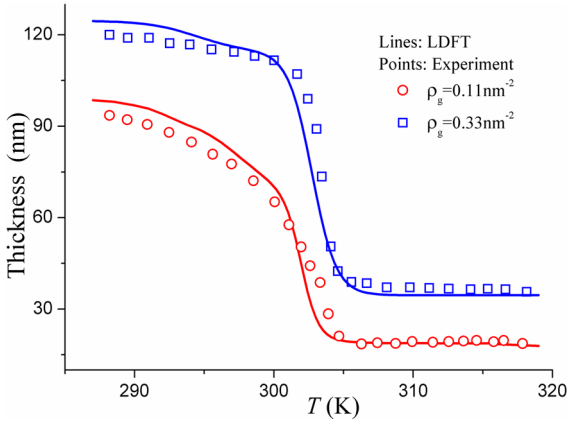

Figure 9. The temperature sensitive swelling behavior of PNIPAM brushes with varying grafting densities. Line: calculated results; the points are experimental results, ○ for grafting density (0.11 nm^{-2}), and □ for grafting density (0.33 nm^{-2}). The swelling ratio of brush 1, which has a higher grafting density (0.33 nm^{-2}) is 3.25, while the value of brush 2 is about 5.0.

increasing grafting density decreases the swelling ratio and LCST of the polymer brush.

4. CONCLUSIONS

The lattice density functional theory developed previously based on the close-packed model is used for studying polymer brushes. We compare the density profiles of polymer segments calculated by LDFT with that of reported molecular simulation results to validate the numerical performance of LDFT, and the results of LDFT are in satisfactory agreement with simulation. Then, the heating-induced swelling behavior of tethered polymer brushes with five different phase diagrams (UCST, LCST, both UCST and LCST, closed LOOP, and hourglass shaped) are discussed, and the correspondence between the phase behavior of polymer solution and the swelling behavior of brush was found. Finally, this correspondence was used to predict the thickness of PNIPAM brushes under different temperatures. Consistent with experiments, the LDFT developed can provide some guidance to the design of thermoresponsive polymer brushes for targeted application.

In essence, the correspondence between bulk polymer solution and inhomogeneous polymer brush stems from the temperature-dependent expression of exchange energy obtained from the double-lattice model.[48−51] More rigorous statistical mechanical treatment of polar interactions such as hydrogen bond is still needed to detail the physical significance of energy parameters, which is already in our present study.

AUTHOR INFORMATION

Corresponding Authors

*E-mail: xqchen@ecust.edu.cn.

*E-mail: hlliu@ecust.edu.cn.

Notes

The authors declare no competing financial interest.

ACKNOWLEDGMENTS

This work is supported by the National Basic Research Program of China (Grant 2014CB748500), the National Natural Science Foundation of China (Grants 91334203, 21306042, and 21176065), the 111 Project of Ministry of Education of China (Grant B08021), the Natural Science Foundation of Shanghai (Grant 13ZR1410800), and the Fundamental Research Funds for the Central Universities.

REFERENCES

(1) Jochum, F. D.; Theato, P. Temperature- and light-responsive smart polymer materials. *Chem. Soc. Rev.* **2013**, *42* (17), 7468.

(2) Roy, D.; Cambre, J. N.; Sumerlin, B. S. Future perspectives and recent advances in stimuli-responsive materials. *Prog. Polym. Sci.* **2010**, *35* (1−2), 278−301.

(3) Stuart, M. A. C.; Huck, W. T. S.; Genzer, J.; Muller, M.; Ober, C.; Stamm, M.; Sukhorukov, G. B.; Szleifer, I.; Tsukruk, V. V.; Urban, M.; Winnik, F.; Zauscher, S.; Luzinov, I.; Minko, S. Emerging applications of stimuli-responsive polymer materials. *Nat. Mater.* **2010**, *9* (2), 13.

(4) Lee, H.-i.; Pietrasik, J.; Sheiko, S. S.; Matyjaszewski, K. Stimuli-responsive molecular brushes. *Prog. Polym. Sci.* **2010**, *35* (1−2), 24−44.

(5) Zhao, B. Synthesis of binary mixed homopolymer brushes by combining atom transfer radical polymerization and nitroxide-mediated radical polymerization. *Polymer* **2003**, *44* (15), 4079−4083.

(6) Li, M.-H.; Keller, P. Stimuli-responsive polymer vesicles. *Soft Matter* **2009**, *5* (5), 927.

(7) Chen, T.; Ferris, R.; Zhang, J.; Ducker, R.; Zauscher, S. Stimulus-responsive polymer brushes on surfaces: Transduction mechanisms and applications. *Prog. Polym. Sci.* **2010**, *35* (1−2), 94−112.

(8) Liu, X.; Ye, Q.; Yu, B.; Liang, Y.; Liu, W.; Zhou, F. Switching water droplet adhesion using responsive polymer brushes. *Langmuir* **2010**, *26* (14), 12377−12382.

(9) Strozyk, M. S.; Chanana, M.; Pastoriza-Santos, I.; Pérez-Juste, J.; Liz-Marzán, L. M. Protein/polymer-based dual-responsive gold nanoparticles with pH-dependent thermal sensitivity. *Adv. Funct. Mater.* **2012**, *22* (7), 1436−1444.

(10) Xu, Y.; Chen, X.; Chen, H.; Xu, S.; Liu, H.; Hu, Y. Density functional theory for the selective adsorption of small molecules on a surface modified with polymer brushes. *Mol. Simul.* **2012**, *38* (4), 274−283.

(11) Bittrich, E.; Burkert, S.; Müller, M.; Eichhorn, K.-J.; Stamm, M.; Uhlmann, P. Temperature-sensitive swelling of poly(*N*-isopropylacrylamide) brushes with low molecular weight and grafting density. *Langmuir* **2012**, *28* (7), 3439−3448.

(12) Yim, H.; Kent, M. S.; Mendez, S.; Balamurugan, S. S.; Balamurugan, S.; Lopez, G. P.; Satija, S. Temperature-dependent

conformational change of PNIPAM Grafted Chains at High Surface Density in Water. *Macromolecules* **2004**, *37* (5), 1994−1997.
(13) Yim, H.; Kent, M. S.; Mendez, S.; Lopez, G. P.; Satija, S.; Seo, Y. Effects of grafting density and molecular weight on the temperature-dependent conformational change of poly(*N*-isopropylacrylamide) grafted chains in water. *Macromolecules* **2006**, *39* (9), 3420−3426.
(14) Zhu, X.; Yan, C.; Winnik, F. M.; Leckband, D. End-grafted low-molecular-weight PNIPAM does not collapse above the LCST. *Langmuir* **2007**, *23* (1), 162−169.
(15) Kent, M. S. A quantitative study of tethered chains in various solution conditions using Langmuir diblock copolymer monolayers. *Macromol. Rapid Commun.* **2000**, *21* (6), 243−270.
(16) Han, X.; Zhang, X.; Yin, Q.; Hu, J.; Liu, H.; Hu, Y. Thermoresponsive diblock copolymer with tunable soluble−insoluble and soluble−insoluble−soluble transitions. *Macromol. Rapid Commun.* **2013**, *34* (7), 574−580.
(17) Plamper, F. A.; Schmalz, A.; Müller, A. H. E. Tuning the thermoresponsiveness of weak polyelectrolytes by pH and light: Lower and upper critical-solution temperature of poly(*N*,*N*-dimethylaminoethyl methacrylate). *J. Am. Chem. Soc.* **2007**, *129* (47), 14538−14539.
(18) Chakrabarti, A.; Toral, R. Density profile of terminally anchored polymer chains: A Monte Carlo study. *Macromolecules* **1990**, *23* (7), 2016−2021.
(19) Lai, P.-Y.; Binder, K. Structure and dynamics of polymer brushes near the Theta point: A Monte Carlo simulation. *J. Chem. Phys.* **1992**, *97* (1), 586−595.
(20) Murat, M.; Grest, G. S. Structure of a grafted polymer brush: A molecular dynamics simulation. *Macromolecules* **1989**, *22* (10), 4054−4059.
(21) Grest, G. S. Grafted polymer brushes: A constant surface pressure molecular dynamics simulation. *Macromolecules* **1994**, *27* (2), 418−426.
(22) Grest, G. S. Interfacial sliding of polymer brushes: A molecular dynamics simulation. *Phys. Rev. Lett.* **1996**, *76* (26), 4979−4982.
(23) Karim, A.; Satija, S. K.; Douglas, J. F.; Ankner, J. F.; Fetters, L. J. Neutron reflectivity study of the density profile of a model end-grafted polymer brush: Influence of solvent quality. *Phys. Rev. Lett.* **1994**, *73* (25), 3407−3410.
(24) Grest, G. S.; Lacasse, M.-D.; Kremer, K.; Gupta, A. M. Efficient continuum model for simulating polymer blends and copolymers. *J. Chem. Phys.* **1996**, *105* (23), 10583−10594.
(25) Lee, S. G.; Pascal, T. A.; Koh, W.; Brunello, G. F.; Goddard, W. A.; Jang, S. S. Deswelling mechanisms of surface-grafted poly(NIPAAm) brush: Molecular dynamics simulation approach. *J. Phys. Chem. C* **2012**, *116* (30), 15974−15985.
(26) Alexander, S. Adsorption of chain molecules with a polar head a scaling description. *J. Phys. (Paris)* **1977**, *38* (8), 983−987.
(27) de Gennes, P. G. Conformations of polymers attached to an interface. *Macromolecules* **1980**, *13* (5), 1069−1075.
(28) Baulin, V. A.; Zhulina, E. B.; Halperin, A. Self-consistent field theory of brushes of neutral water-soluble polymers. *J. Chem. Phys.* **2003**, *119* (20), 10977−10988.
(29) Wijmans, C. M.; Zhulina, E. B. Polymer brushes at curved surfaces. *Macromolecules* **1993**, *26* (26), 7214−7224.
(30) Müller, M. Phase diagram of a mixed polymer brush. *Phys. Rev. E* **2002**, *65* (3), 030802.
(31) Milner, S. T.; Witten, T. A.; Cates, M. E. Theory of the grafted polymer brush. *Macromolecules* **1988**, *21* (8), 2610−2619.
(32) Zhulina, E.; Balazs, A. C. Designing patterned surfaces by grafting Y-shaped copolymers. *Macromolecules* **1996**, *29* (7), 2667−2673.
(33) Mendez, S.; Curro, J. G.; McCoy, J. D.; Lopez, G. P. Computational modeling of the temperature-induced structural changes of tethered poly(N-isopropylacrylamide) with self-consistent field theory. *Macromolecules* **2004**, *38* (1), 174−181.
(34) Ma, X.; Chen, C.; Tang, P.; Qiu, F. SCFT study of microphase separation in mixed polymer brushes grafted on cylindrical surface. *Acta Chimica Sinica* **2014**, *72* (2), 208−214.
(35) Gong, K.; Chapman, W. G. Solvent response of mixed polymer brushes. *J. Chem. Phys.* **2011**, *135* (21), 214901.
(36) Gong, K.; Marshall, B. D.; Chapman, W. G. Response behavior of diblock copolymer brushes in explicit solvent. *J. Chem. Phys.* **2012**, *137* (15), 154904.
(37) Xu, Y.; Chen, X.; Han, X.; Xu, S.; Liu, H.; Hu, Y. Lock/unlock mechanism of solvent-responsive binary polymer brushes: Density functional theory approach. *Langmuir* **2013**, *29* (16), 4988−4997.
(38) Gong, K.; Marshall, B. D.; Chapman, W. G. Modeling lower critical solution temperature behavior of associating polymer brushes with classical density functional theory. *J. Chem. Phys.* **2013**, *139*, 094904.
(39) Chen, Y.; Aranovich, G. L.; Donohue, M. D. Liquid−vapor density profiles from equilibrium limit of diffusion equation for interacting particles. *J. Colloid Interface Sci.* **2007**, *307* (1), 34−39.
(40) Chen, Y.; Aranovich, G. L.; Donohue, M. D. Thermodynamics of symmetric dimers: Lattice density functional theory predictions and simulations. *J. Chem. Phys.* **2006**, *124* (13), 134502−134508.
(41) Chen, X.; Sun, L.; Liu, H.; Hu, Y.; Jiang, J. A new lattice density functional theory for polymer adsorption at solid-liquid interface. *J. Chem. Phys.* **2009**, *131* (4), 044710.
(42) Men, Y.; Zhang, X. Physical basis for constrained lattice density functional theory. *J. Chem. Phys.* **2012**, *136* (12), 124704−124707.
(43) Yang, J.; Xin, Q.; Sun, L.; Liu, H.; Hu, Y.; Jiang, J. A new molecular thermodynamic model for multicomponent Ising lattice. *J. Chem. Phys.* **2006**, *125* (16), 164506.
(44) Yang, J.; Yan, Q.; Liu, H.; Hu, Y. A molecular thermodynamic model for binary lattice polymer solutions. *Polymer* **2006**, *47* (14), 5187−5195.
(45) Yang, J.; Peng, C.; Liu, H.; Hu, Y. Liquid−liquid equilibria of polymer solutions with oriented interactions. *Fluid Phase Equilib.* **2006**, *249* (1−2), 192−197.
(46) Guggenheim, E. A.; McGlashan, M. L. Entropies of mixing in certain athermal binary solutions. *Proc. R. Soc., Ser. A* **1950**, *203* (1075), 435−454.
(47) Laradji, M.; Guo, H.; Zuckermann, M. J. Off-lattice Monte Carlo simulation of polymer brushes in good solvents. *Phys. Rev. E* **1994**, *49* (4), 3199−3206.
(48) Hu, Y.; Ying, X.; Wu, D. T.; Prausnitz, J. M. Molecular thermodynamics of polymer solutions. *Fluid Phase Equilib.* **1993**, *83* (0), 289−300.
(49) Hu, Y.; Liu, H.; Shi, Y. Molecular thermodynamic theory for polymer systems. I. A close-packed lattice model. *Fluid Phase Equilib.* **1996**, *117* (1−2), 100−106.
(50) Hu, Y.; Lambert, S. M.; Soane, D. S.; Prausnitz, J. M. Double-lattice model for binary polymer solutions. *Macromolecules* **1991**, *24* (15), 4356−4363.
(51) Hu, Y.; Liu, H.; Soane, D. S.; Prausnitz, J. M. Binary liquid-liquid equilibria from a double-lattice model. *Fluid Phase Equilib.* **1991**, *67* (0), 65−86.
(52) Lian, C.; Zhi, D.; Xu, S.; Liu, H.; Hu, Y. A lattice model for thermally-sensitive core-shell hydrogels. *J. Colloid Interface Sci.* **2013**, *406*, 148−153.
(53) Zhi, D.; Lian, C.; Xu, S.; Huang, Y.; Liu, H. Molecular thermodynamic model for swelling and volume phase transition behavior of random copolymer gels. *CIESC J.* **2013**, *64* (1), 268−274.
(54) Afroze, F.; Nies, E.; Berghmans, H. Phase transitions in the system poly (< i> N</i>-isopropylacrylamide)/water and swelling behaviour of the corresponding networks. *J. Mol. Struct.* **2000**, *554* (1), 55−68.